Desalination 404 (2017) 22–34

Contents lists available at ScienceDirect

Desalination

journal homepage: www.elsevier.com/locate/desal

Experimental and theoretical investigations on water desalination using direct contact membrane distillation

A. Khalifa [a,*], H. Ahmad [a], M. Antar [a], T Laoui [a], M. Khayet [b,c]

[a] Mechanical Engineering Department, King Fahd University of Petroleum & Minerals, Dhahran 31261, Saudi Arabia
[b] Department of Applied Physics I, Faculty of Physics, University Complutense of Madrid, Av. Complutense s/n, 28040 Madrid, Spain
[c] Madrid Institute for Advanced Studies of Water (IMDEA Water Institute), Calle Punto Com No. 42, Alcalá de Henares, 28805 Madrid, Spain

HIGHLIGHTS

- Comprehensive experimental and theoretical studies on DCMD system
- Effects of main operating variables and membrane degradation
- Theoretical results agree with experimentally measured values.
- Membrane characterization and SEM micrographs before and after use
- Evaporation efficiency and GOR values are calculated for energy efficiency.

ARTICLE INFO

Article history:
Received 12 July 2016
Received in revised form 10 October 2016
Accepted 14 October 2016
Available online 2 November 2016

Keywords:
Water desalination
Direct contact membrane distillation
Performance investigation
Experimental and theoretical studies
Membrane characterization and degradation

ABSTRACT

Direct contact membrane distillation (DCMD) is one of the commonly used configurations of membrane distillation technology for water desalination. In the present study, comprehensive investigations on different parameters affecting the performance of the DCMD system are presented. The investigated variables include the hot feed and the cold permeate temperatures, feed-permeate temperature difference and ratio, feed and permeate flow rates, feed-permeate flow rate ratio, feed concentration, membrane pore size, and membrane degradation with time, etc. An analytical model, based on the heat and mass transfer equations within the DCMD module, was used to predict the system performance at different operating conditions. The model was used to predict the temperature difference across the membrane surfaces and then calculating the vapor pressure difference leading to the permeate flux. The model was validated with the experimental measurements. The permeate flux increases with increasing the feed temperature, feed flow rate, permeate flow rate, and pore size, and decreases with increasing the permeate temperature and feed concentration. The productivity of the system is very promising since a permeate flux of 100 kg/m^2·h was achieved at 90 °C for hot feed side and 5 °C for cold side stream. The DCMD system is able to handle feeds with high salt concentration of 100 g/L with remarkably high salt rejection factor and low permeate total dissolved solids (TDS). The SEM micrographs showed the used polytetrafluoroethylene (PTFE) membrane covered with a fouling layer, as compared to the as-received membrane, which attests the need for feed pretreatment and/or membrane washing to recover the membrane performance. The evaporative (thermal) efficiency ranged from 70% to 95% and the GOR values ranged from 0.8 to 1.2 corresponding to feed temperature from 40 °C to 90 °C, depending mainly on the feed temperature.

1. Introduction

Many countries worldwide suffer from real water shortage caused by the rapid population growth, economic development, and diminishing nature water resources. Projections increase of >2% in fresh water demand has been reported in many countries which is almost double their population growth rates [1]. It is predicted that some regions of the world will be plagued by water scarcity [2–5] mainly due to the economic growth and development. Shortage of fresh water can be solved by desalination processes in which substantial amount of energy to be used [6,7]. Presently, 50% of the world's total desalination capacity is based on membrane using the concept of reverse osmosis, and the remaining shares are by thermal processes such as the multi-stage flashing (MSF), the multi effect desalination (MED), vapor compression (VC) and adsorption desalination (AD). The

* Corresponding author.
E-mail address: akhalifa@kfupm.edu.sa (A. Khalifa).

http://dx.doi.org/10.1016/j.desal.2016.10.009
0011-9164/

thermally-based (non-membrane) desalination methods are dominantly used in the Arab Gulf Cooperation Council (GCC) countries [8, 9]. The major reasons for adopting the thermal methods in the GCC countries are; firstly, the high feed salinity in the Gulf and the fouling susceptibility of membranes at high brine concentration limits the water recovery ratio of RO process. Secondly, the frequent occurrences of harmful algae blooms (HABs) in the water of Gulf tend to contain high concentration of toxins in seawater feed that may pass through the membrane pores, causing human illnesses and death if the toxins are ingested [3].

There is a rapid growth in using membrane technologies for water desalination. Membrane distillation (MD) is one of those technologies that have a potential and can be applied to produce distillate water from seawater and brackish water. It involves a hydrophobic microporous membrane that separates water vapor from the salty feed water. Hydrophobicity of membrane disallows water in liquid form because of surface tension but vapor can pass through. The driving force of permeation across the membrane is the vapor partial pressure difference of the two streams on the membrane sides, which is a function of the temperature difference across the membrane. In direct contact membrane distillation (DCMD) design, vaporization takes place at the liquid-vapor interface at the membrane pore surface in the feed side. Vapor is then permeates through the pores from the hot side to the cold side due to the difference in vapor pressure across the membrane (capillary action). The permeated vapor is then condensed in the cold stream side of the membrane [10]. DCMD is not only limited to water purification but can also be used for treatment of very high concentrations such as oilfield produced water [11]. Macedonio et el. reported that a good salt rejection factor can be obtained by desalinating water that is obtained after oilfield treatment by using Polypropylene (PP) and polyvinydene fluoride (PVDF) membranes at high flow rates of feed and coolant. Manawi et al. [12] determined the effect of temperature polarization on the permeate flux by measuring intermediate temperatures on membrane surface. They developed a multi-dimensional model in order to estimate temperatures at different points on membrane surface, and optimized the permeate flux by minimizing temperature polarization coefficient. The effect of feed water salinity was studied by Hsu et al. [13], using a NaCl-H_2O solution and seawater as feeds. They compared the performances of both systems, and they used ultrasonic technique for cleaning purpose.

Boubakri et al. [14] performed DCMD experiments using PP membrane with a low pore size of 0.064 μm. They reported that the permeate flux reached 4.24 L/m^2 h at a temperature difference of 60 °C and Reynolds number (*Re*) of 3740. Lin et al. [15] presented a comprehensive energy analysis of MD-HX system and defined optimum relative flow rates, mass recovery rates, and specific heat duty for the system. They coupled MD module with a heat exchanger in order to recover latent of condensation of vapors in the coolant stream using a circular module. Srisurichan et al. [16] investigated the mass transport and fouling mechanism in DCMD system. They suggested that molecular diffusion model was the best one for diffusion in fouling related phenomenon. The effect of coolant velocity is not well explained in literature. Some researchers have a point of view of decreasing flux by increasing permeate velocity while others have an opposite viewpoint. Naidu et al. [17] reported that a velocity ranging between 0.8 and 1.2 m/s was optimum for feed and permeate sides. Ho et.al. [18] studied the effect of channel smoothness and flow direction and used eddy promoter to make roughened surface channels for feed and permeate. They reported that the counter-current direction flow resulted in higher permeate flux than concurrent flow arrangement. Qtaishat et al. [19]. presented a detailed analysis of the heat transfer in DCMD through a mathematical model. The coupled effect of mass and heat transfers was addressed and an experimental validation was presented. Performance indicators such as the temperature polarization coefficient, the membrane mass transfer coefficient and the evaporation efficiency were discussed. Andrjesdóttir [10] investigated a different forms of dusty gas model utilized for mass transfer. Different heat and mass transfer correlations were tested, and the transitional model was found to give the best correlation. The model was also used by Dahiru and Khalifa [20]. Depending upon the pore size, a three-parameter model namely Knudsen diffusion, Molecular diffusion, and Poiseullie flow is considered. Transition model (KMPT) was introduced by Ding et al. [21] to predict membrane distillation coefficient. For large pores, dominating Poiseullie flow was observed. Therefore, two or three of the three mechanisms (Knudsen, molecular, Poiseullie) could be present in a single membrane. Martinez and Diaz [22] developed a model depending on dusty gas model of gas transport through membrane pores. The model showed a good agreement with the experimental values.

In this paper, a comprehensive study on the main variables affecting the DCMD performance and degradation is presented, both experimentally and analytically. The investigated variables included feed temperature, cold permeate temperature, feed-to-permeate temperature difference and ratio, feed flow rate, permeate flow rate, feed-to-permeate flow rate ratio, feed concentration up to 100 g/L, membrane pore size, and membrane degradation with time. The membranes used were characterized and the effects of continuous operation on the membrane surface and system performance were investigated. The analytical model is based on solving the equations of heat and mass transfer within the DCMD module.

2. Mathematical modelling

2.1. Mass transfer

Fig. 1 shows the configuration of DCMD module. The hot feed stream flows over a hydrophobic membrane. On the other side of the membrane, cold permeate flows. The temperature difference between the membrane surfaces creates a difference of vapor pressure across the membrane that causes feed vapor permeate through membrane pores, and condense on the cold permeate side.

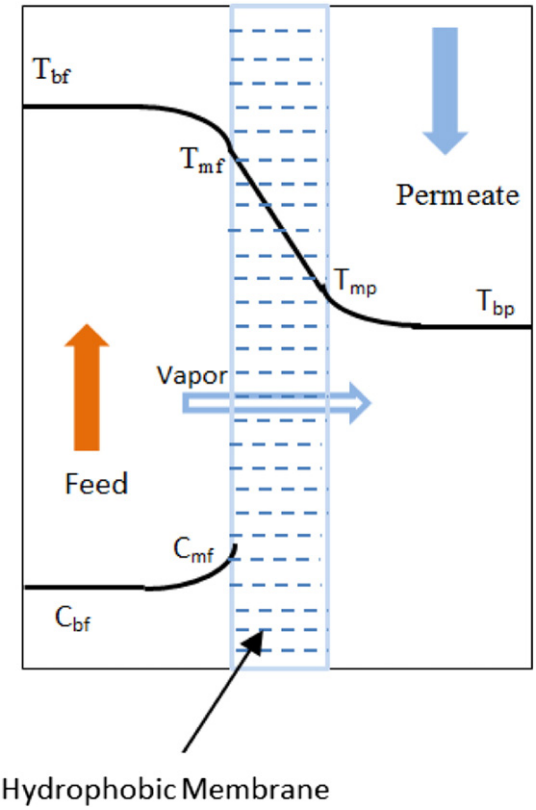

Fig. 1. Schematic of DCMD process with temperature and concentration variations.

The permeate mass flux through the membrane depends mainly on the difference of vapor pressure of water in feed and permeate sides. The permeate mass flux can be given as [23–25];

$$J_w = D_e * \Delta p_m = D_e * \left(P^o{}_{wf} - P^o{}_{wp}\right) \tag{1}$$

where J_w is the mass flux of permeate, and D_e is the equivalent diffusion coefficient. ΔP_m is the vapor pressure difference at transmembrane surfaces. $P^o{}_{wf}$ and $P^o{}_{wp}$ are the vapor pressures of feed and permeate sides at the membrane surfaces; respectively, and are calculated from Antoine equation as follows:

$$p^0{}_{wf} = \exp\left((23.1964) - \frac{3816.44}{T_{mf} - 46.13}\right) \tag{2}$$

$$p^0{}_{wp} = \exp\left((23.1964) - \frac{3816.44}{T_{mp} - 46.13}\right) \tag{3}$$

If we consider the effect of salinity in the feed solution then Eq. (1) is written as,

$$J_w = D_e * \left(p^o{}_{wf} * \gamma_{wf} * x_{wf} - p^o{}_{wp}\right) \tag{4}$$

where γ_{wf} is activity coefficient and x_{wf} is the mole fraction of water in feed. The activity coefficient represents the variation of substances from their ideal behavior due to impurities, and mole fraction is the ratio of numbers of moles of any specie to the total number of moles present in solution.

For an aqueous solution of NaCl, the activity co-efficient is given as [24,26–28]

$$\gamma_{wf} = 1 - (0.5 * x_{NaCl}) - (10 * x^2{}_{NaCl}) \tag{5}$$

where x_{NaCl} is the mole fraction of NaCl in water solution.

Essalhi et al. [24] considered the combined effect of Knudsen and molecular diffusions by introducing a factor α which is the ratio of Knudsen diffusion to mass diffusion and shows the dominance of phenomenon which is occurring in mass transfer. The value of α can vary between 0 and 1,

$$D_e = \left(\left(\frac{\alpha}{D_k}\right) + \left(\frac{1-\alpha}{D_m}\right)\right)^{-1} \tag{6}$$

D_k and D_m represent Knudsen and molecular diffusion coefficients; respectively, and can be found by the following expressions,

$$D_k = \left(\left(\frac{3 * \delta * \tau}{2 * \varepsilon * d_{pore}}\right) * \left(\frac{\pi * R * T_m}{8 * Mol_w}\right)^{0.5}\right)^{-1} \tag{7}$$

$$D_m = \left(\frac{R * T_m * \delta * \tau * P_{air,pore}}{Mol_w * \varepsilon * PD_{w,a}}\right)^{-1} \tag{8}$$

where δ is the membrane thickness, ε is the membrane porosity, R is the universal gas constant, T_m is the mean or average temperature across membrane surfaces, d_{pore} is the pore diameter, Mol_w is the molecular weight of water molecules, P is the total pressure inside the pore, and $D_{w,a}$ is pressure independent molecular diffusion coefficient for water and air or simply the diffusivity of water vapors in air.

τ is the membrane tortuosity which is given as [29];

$$\tau = \frac{1}{\varepsilon} \tag{9}$$

Diffusivity of water vapors produced through the static air inside the membrane pores can be calculated as [10,28,30];

$$PD_{w,a} = 1.895 \times 10^{-5} \cdot T_m{}^{2.072} \tag{10}$$

The total pressure inside the pores is assumed to be the average of feed and permeate side pressures; that is:

$$P_{pore} = \frac{P_f + P_p}{2} \tag{11}$$

Considering air and water vapors filling the pores then the partial pressure of air inside the membrane pores can be written as,

$$P_{air,pore} = P_{pore} - P_{w,v,p} \tag{12}$$

where $P_{w,v,p}$ represents the partial pressure of water vapors inside the pores which can be calculated using.

Antoine equation based on the mean temperature across the membrane surfaces, T_m, where

$$T_m = \frac{T_{mf} + T_{mp}}{2} \tag{13}$$

2.2. Heat transfer

Referring to DCMD configuration in Fig. 1, different modes of heat transfer are identified. In the feed side, fluid is at high temperature, high salinity flowing over the membrane surface. The heat transfer in this side will be due to convection. Then on the permeate side the fluid is flowing, causing convective heat transfer to occur. Through the membrane, the heat transfer is due conduction and mass flux. Thus, heat transfer in a DCMD module is occurring in three regions.

(1) Convective heat transfer (Q, W/m^2) from the feed stream to membrane surface, governed by Newton's law of cooling [18, 24,30],

$$Q_f = h_f * \left(T_{bf} - T_{mf}\right) \tag{14}$$

where T_{bf} and T_{mf} are the feed temperature and membrane surface temperature in the feed side respectively. h_f is the convective heat transfer coefficient in feed side that can be calculated by using different correlations depending on the flow type (laminar or turbulent).

(2) Heat transfer through membrane material by conduction and through the pores by evaporative mass flux.

Heat carried by the vapors (Evaporative heat transfer) is written as product of vapor mass flux (J_w) and enthalpy of vaporization (ΔH_v);

$$Q_v = J_w * \Delta H_v \tag{15}$$

The Enthalpy of vaporization of water is taken as [31]

$$\Delta H_v = \left((1.7535 * T_{mf}) + 2024.3\right) \tag{16}$$

where T_{mf} is the temperature of the membrane surface at feed side. Conductive heat transfer through membrane matrix is calculated using Fourier's law of conduction as;

$$Q_c = \left(\frac{k_m}{\delta}\right) * \left(T_{mf} - T_{mp}\right) \tag{17}$$

where T_{mf} and T_{mp} are membrane surface temperatures in feed and permeate side respectively. δ is membrane thickness and k_m is effective

thermal conductivity of membrane. The membrane conductivity can be better predicted on volume average of both gas and polymer conductivities [30,32]. Using isostress series model to determine the thermal conductivity of membrane matrix, the following relation can be considered [30,33].

$$k_m = \left(\left(\frac{\varepsilon}{k_{gas}}\right) + \left(\frac{1-\varepsilon}{k_{mem}}\right)\right)^{-1} \tag{18}$$

The total heat transfer across the membrane is simply the addition of the conductive and evaporative heat transfer through the membrane.

$$Q_m = Q_c + Q_v \tag{19}$$

(3) Convective heat transfer in boundary layer region from membrane surface to permeate stream;

$$Q_p = h_p * (T_{mp} - T_{bp}) \tag{20}$$

where T_{mp} is membrane surface temperature at permeate side, T_{bp} is the permeate stream temperature, and h_p is the convective heat transfer coefficient in permeate side that can be calculated by using different correlations. Under steady state condition, the following conservation of energy is valid,

$$Q_f = Q_m = Q_p \tag{21}$$

The temperatures of the membrane surfaces at feed and permeate sides are calculated as [24,27] ;

$$T_{mf} = \frac{k_m * \left(T_{bp} + \frac{h_f}{h_p} * T_{bf}\right) + ((\delta * (h_f * T_{bf} - J_w * \Delta H_v)))}{(k_m) + \left(h_f * \left(\delta + \left(\frac{k_m}{h_p}\right)\right)\right)} \tag{22}$$

$$T_{mp} = \frac{k_m * \left(T_{bf} + \frac{h_p}{h_f} * T_{bp}\right) + ((\delta * (h_p * T_{bp} + J_w * \Delta H_v)))}{(k_m) + \left(h_p * \left(\delta + \left(\frac{k_m}{h_f}\right)\right)\right)} \tag{23}$$

The values of these temperatures can be inserted back in Eqs. (2) and (3) to determine the vapor pressures and then calculate the flux from Eqs. (1) or (4).

To account for the effect of feed concentration on permeate flux, we define the concentration polarization coefficient as the ratio of salt concentration at the membrane surface to the concentration of salt in the feed stream [24],

$$\beta = \frac{C_{mf}}{C_{bf}} \tag{24}$$

Whereas the concentration at membrane surface is calculated as [31, 33];

$$C_{mf} = C_{bf} * exp\left(\frac{J_w}{k_s * \rho_{bf}}\right) \tag{25}$$

where ρ_{bf} is the density of feed stream and k_s is the solute mass transfer coefficient for the diffusive mass transfer through the concentration boundary layer in the feed side and can be calculated as

$$k_s = Sh * \frac{D_e}{D_h} \tag{26}$$

where D_h is hydraulic diameter of feed channel and Sh is the Sherwood number. Sherwood number is a dimensionless parameter representing the ratio of convective to diffusive mass transport, and it is a function of Reynolds number and Schmidt number. It is analogous to Nusselt number which is used for convective heat transfer [31]. For Laminar flow, Sherwood number is given by Graetz–Lévêque equation [31,34,35]

$$Sh = 1.86 * \left(\mathrm{Re} * Sc * \frac{D_h}{L}\right)^{1/3} \tag{27}$$

where Re is the Reynolds number of the channel flow, the channel flow (internal flow) is laminar if $Re < 2300$ and is turbulent if $Re > 2300$. L is the channel length.

Sc is the Schmidt number, which is the ratio of momentum diffusivity to the mass diffusivity;

$$Sc = \frac{\mu_{mf}}{\rho_{bf} * D_e} \tag{28}$$

where μ_{mf} is the feed viscosity at membrane surface.

For Turbulent flow, Sherwood number is calculated using Dittus–Boelter equation [31]

$$Sh = 0.023 * (Re_f)^{0.8} * (Sc)^{0.33} \tag{29}$$

By definition, the convective heat transfer coefficient is calculated as;

$$h = \frac{Nu * k}{D_h} \tag{30}$$

where k is the average thermal conductivity of fluid in feed or permeate sides, D_h is the hydraulic diameters of flow channels, and Nu is the dimensionless Nusselt number. In case of laminar channel flow, Graetz-Lévéque proposed the following correlation for Nusselt Number [35,36], which is valid for flows in both feed and permeate sides:

$$Nu = 1.86 * \left(\frac{Re * Pr * D_h}{L}\right)^{0.33} \tag{31}$$

where D_h is the channel hydraulic diameter, L is the channel length, and Pris Prandtl number; which is the ratio of viscous diffusion rate to thermal diffusion rate and is defined as;

$$\mathrm{Pr} = \frac{\nu}{\alpha} = \frac{\mu * c_p}{k} \tag{32}$$

where μ is the dynamic viscosity, k is the thermal conductivity, and C_p is the specific heat of the fluid.

In case of turbulent channel flow, the correlations for Nusselt number of the feed (hot side) and permeate (cold side) streams can be given as [24,37];

$$Nu_f = 0.027 * (Re_f)^{0.8} * (Pr_f)^{0.4} * \left(\left(\frac{\mu_{bf}}{\mu_{mf}}\right)\right)^{0.14} \tag{33}$$

$$Nu_p = 0.027 * (Re_p)^{0.8} * (Pr_p)^{0.33} * \left(\left(\frac{\mu_{mp}}{\mu_{bp}}\right)\right)^{0.14} \tag{34}$$

The total heat transfer in the module membrane can be written in terms of the overall heat transfer coefficient, U, as

$$Q_m = U * (T_{bf} - T_{bp}) \tag{35}$$

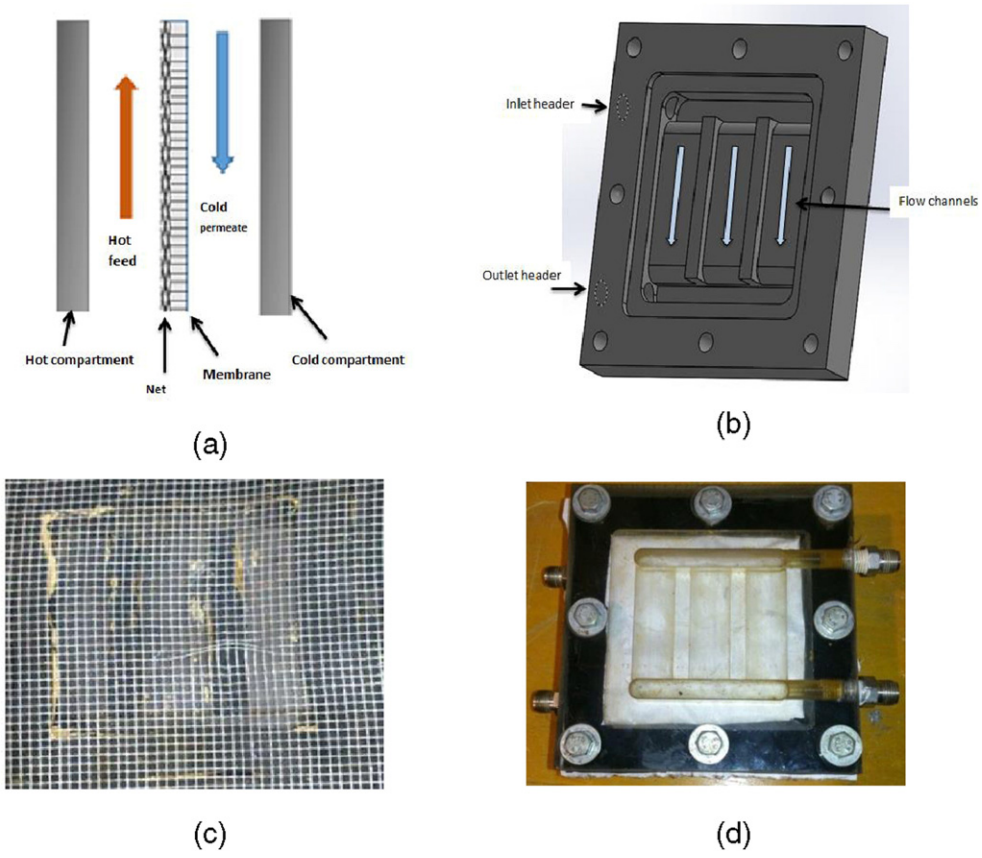

Fig. 2. Design and assembly of the DCMD module; (a) module assembly, (b) module flow channels (c) membrane supporting mesh spacer, (d) assembled module.

The overall heat transfer coefficient is based on the difference in temperatures between feed and permeate streams and can be determined as follows [38];

$$U = \left[\frac{1}{h_f} + \frac{1}{\left(\frac{k_m}{\delta}\right) + \frac{J_w \cdot \Delta H_v}{(T_{mf} - T_{mp})}} + \frac{1}{h_p}\right]^{-1} \tag{36}$$

3. Experimental setup

The DCMD module consists of a flat-sheet membrane and a channeled MD module. The module is made up of two Plexiglas flow compartments [39]. Fig. 2a shows the module assembly where the membrane is sandwiched between the two flow compartments. Each flow compartment has dimensions of 160 mm long, 160 mm wide, and 25 mm thick as shown in Fig. 2b. One compartment is used for hot feed water; while the other compartment is used for permeate cold water. Water enters through header and distributed into three channels. After passing over the membrane surface, the fluid is collected back into the exit header. Each flow compartment has three rectangular channel of the same dimensions of 66 mm in length, 24 mm in width and 5 mm in depth. A feed spacer, in the form of a mesh (net), is used between the feed stream and active side of membrane surface, as shown in Fig. 2c. The purpose of this spacer is to mechanically support the membrane in addition to enhance the turbulence level in the feed channel for better permeation flux. To avoid internal leakage, a rubber sheet of 2 mm thickness is used as a gasket.

Internal leakage may happen because of membrane rupture at sharp edges during the module assembly. The assembled module is shown in Fig. 2d. The effective membrane area of permeation is $6.192E-2\ m^2$. Insulated steel pipes are used for inlet and outlet fluid transmission from heater and chiller. The water heater and chiller operate by controlled thermostat head (acquired from ThermoFisher), and are used to provide constant flow rates and constant temperatures for the feed and coolant streams. A float flow meter is used to measure feed flow rate and a turbine flow meter is used to measure coolant flow rate. The feed and the permeate concentrations are measured using a calibrated conductivity meter. Pressure gauges (max range of 2 bar) are used to measure and observe the inlet and outlet pressure of feed and permeate sides. Hi-Speed USB Carrier (National Instruments) is used for data acquisition. K-type thermocouples are used to monitor the inlet and outlet temperature of feed and permeate sides. The extra permeate is collected from the chiller tank with time via a tube at its top. Fig. 3 shows a real photo of the instrumented DCMD module and a schematic of the experimental setup.

In the experimental work, four levels of feed concentrations are tested: (1) Sweet tap water having concentration of 0.140 g/L, (2) Aqueous salt NaCl solution of 2 g/L, (3) Seawater collected from Arabian Gulf, Al-Khobar, Kingdom of Saudi Arabia with 43 g/L salt concentration (without any pre-treatment), and (4) Extreme lab NaCl-water salt solution of 100 g/L.

4. Results and discussion

The current investigation aimed to present a comprehensive experimental and analytical study on the variables that affect the performance of the DCMD system. In this section, the feed temperature is varied from 40 to 90 °C. The cold permeate temperature is varied from 5 °C to 25 °C. The feed flow rate and coolant flow rate are tested at three different levels. Different concentrations of the feed water of 0.14, 2, 43 and 100 g/L are examined. PTFE membranes having two different mean pore sizes of 0.45 μm and 0.22 μm are used.

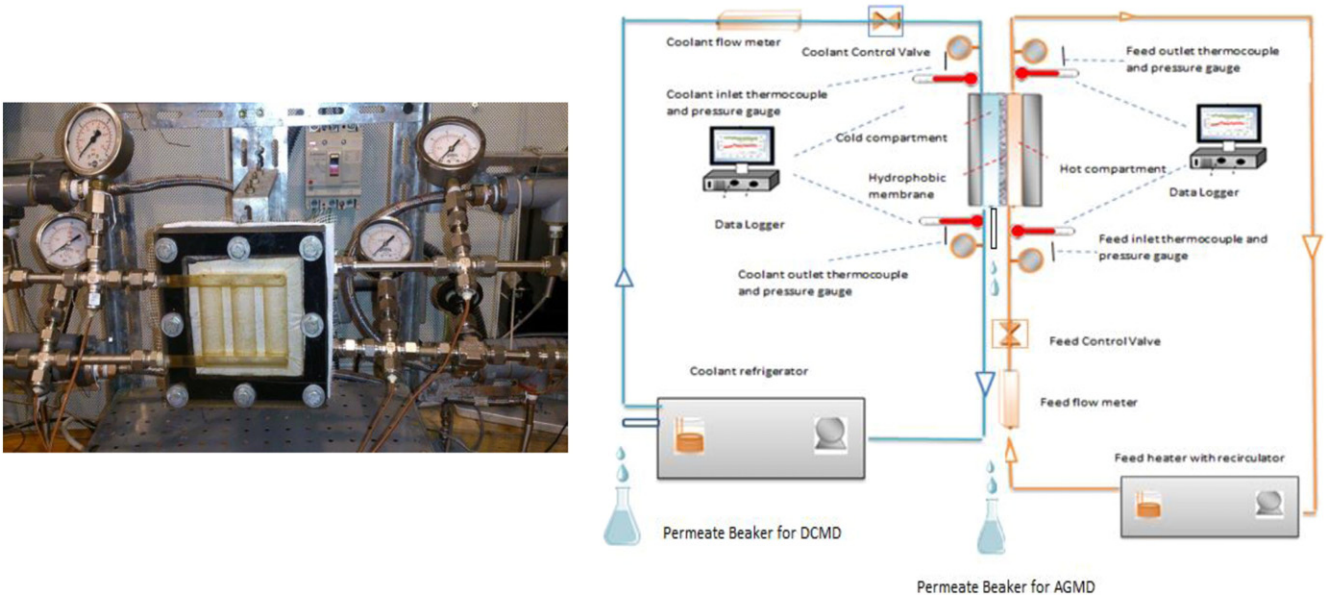

Fig. 3. The Instrumented DCMD module and a schematic diagram of the experimental setup.

4.1. Effect of feed and permeate temperatures

The effects of feed temperature on the permeate flux are studied over a range of temperatures from 40 °C to 90 °C with an increment of 10 °C. The flux change with feed temperature was observed at varying cold permeate temperatures of 5 °C, 10 °C, 15 °C, 20 °C, and 25 °C; respectively, with feed concentration of 2 g/L. Experimental and theoretical results are shown in Fig. 4(a) to (e) as separate sub-figures to avoid data clustering and to shed more light on the validation of the theoretical model. Increasing the feed temperature increases the permeate flux,

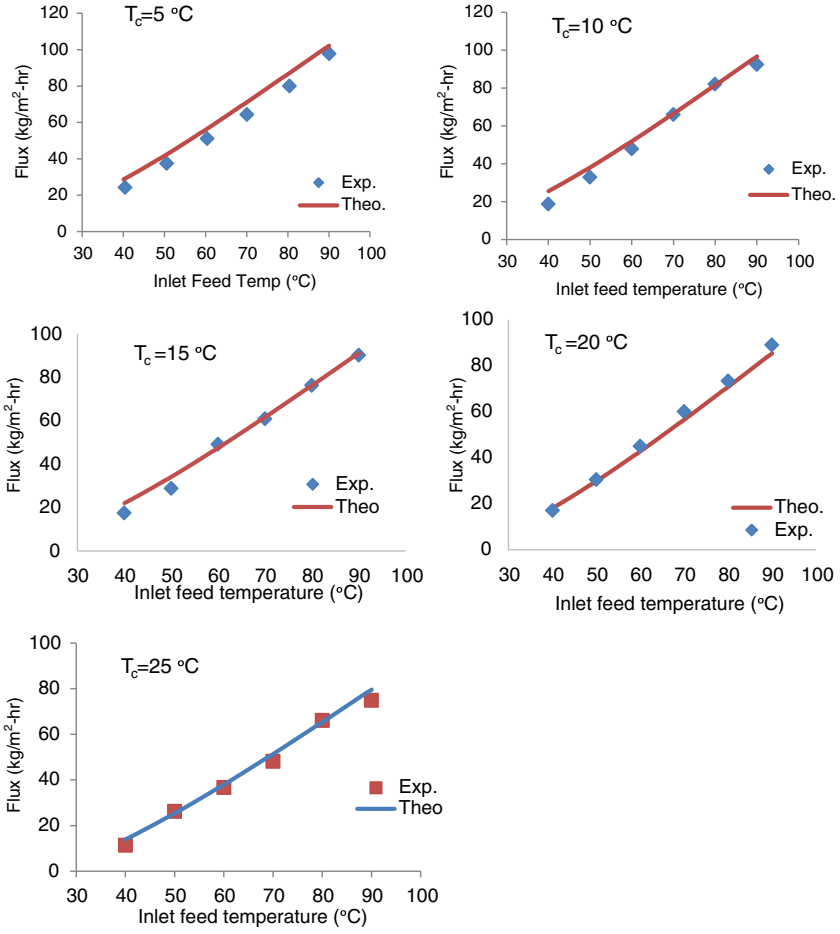

Fig. 4. Effect of feed temperature on permeate flux at different cold permeate temperatures. *Conditions*: membrane PTFE 0.45 μm, feed concentration 2 g/L, feed flow rate 4.6 L/min, coolant flow rate 3.65 L/min.

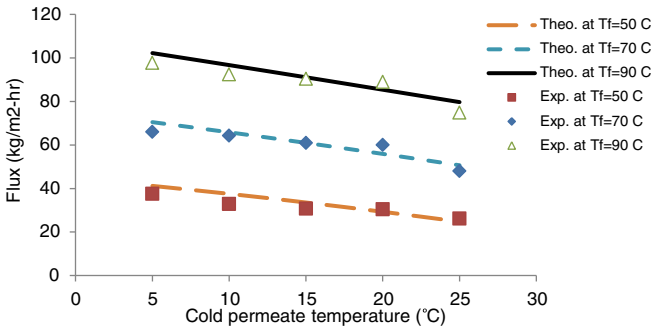

Fig. 5. Effect of cold permeate temperature on permeate flux Conditions: membrane PTFE 0.45 μm, feed salinity 2 g/L, feed flow rate 4.6 L/min, cold permeate flow rate 3.65 L/min.

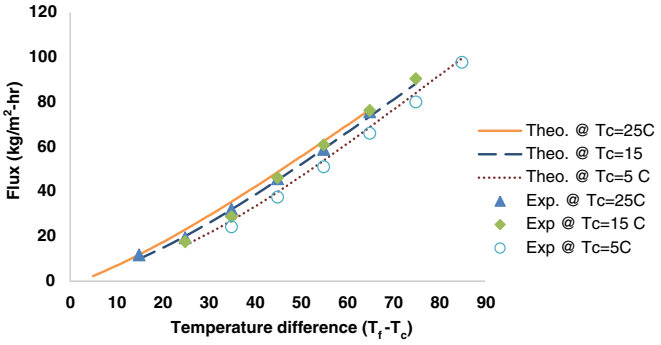

Fig. 7. Effect of operating temperature difference on flux.

almost in an exponential way in agreement with Antoine Eq. (2). According to this equation, the effect of temperature on vapor pressure is small at low feed temperature, and becomes very significant at high feed temperature. The maximum permeate flux achieved at feed temperature of 90 °C and cold permeate temperature of 5 °C is about 100 $kg/m^2 \cdot h$. This high value of permeate flux is attributed to the high temperature difference across the membrane, the high porosity of the PTFE membrane, high contact angle, and large pore size. Increasing the temperature difference across the membrane increases the vapor pressure difference between the membrane sides. However, the thermal boundary layer increases and consequently the temperature polarization over the membrane.

The theoretical model predictions of the permeate flux are in good agreement with the experimentally measured values at different temperatures. Maximum deviations between calculated and measured fluxes are found at the lowest permeate temperature of 5 °C. The effect of cold permeate temperature on flux is shown Fig. 5, where the permeate temperature is varied from 5 °C to 25 °C by an increment of 5 °C, at selected feed temperatures. The flux increases as the cold permeate temperature decreases. Decreasing the permeate temperature increases the transmembrane vapor pressure difference; which leads to increasing the permeate flux. The model prediction of flux shows good agreement with the measured values.

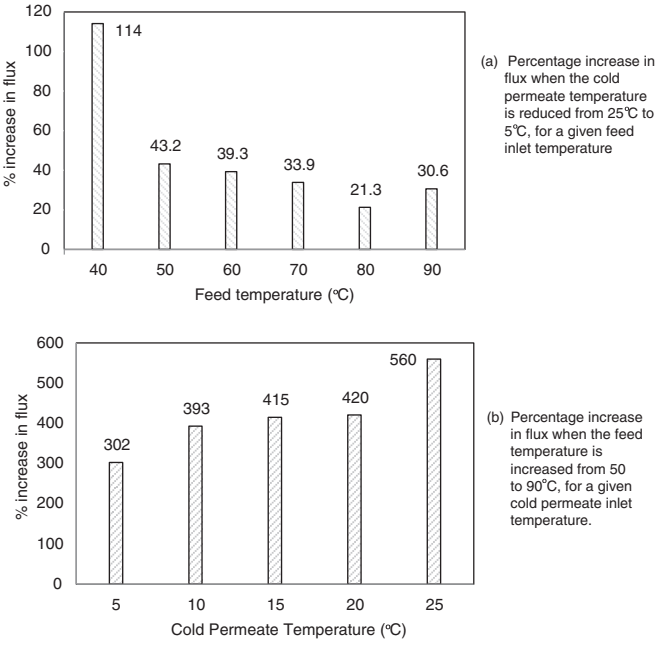

Fig. 6. Percentage increase in flux due to changing the operating temperatures.

In order to assess the effects of operating the DCMD system at different temperatures, the percent change in measured flux is displayed in Fig. 6. Comparatively, from Fig. 6 (a) and (b), increasing the feed stream temperature is more effective in increasing the system flux as compared to decreasing the cold permeate stream temperature. Referring to Fig. 6a, the percentage increase in flux is reported at the corresponding feed temperatures when the cold permeate temperature is reduced from 25 °C to 5 °C. This plot enables us to monitor and justify the effectiveness of cooling the permeate stream down to 5 °C, which consumes a lot of energy, compared to the use of near room temperature permeate stream. In general, reducing the temperature of the cold permeate stream improves the system flux at any given feed temperature. One can report about 35% increase in flux, on average, when reducing permeate temperature from 25 °C to 5 °C, except for feed temperature of 40 °C where the flux increase is significant (114%). Percentagewise, operating at lower permeate temperature is more effective in increasing the flux at low feed temperatures. On the other hand, Fig.6b shows the percentage increase in flux when the feed temperature increases from 50 to 90 °C, at a given temperature of the cold permeate stream. Increasing the feed temperature from 50 to 90 °C increases the flux by 302 to 560%, depending on the temperature of cold permeate stream. However, the percentage increase in flux increases with increasing the cold permeate temperature. It may be understood that although operating the DCMD system at low permeate temperature can yield higher values of flux, the percentage increase in flux is larger at high permeate temperature, for the same range of increased feed temperature.

Since the operating temperatures for feed (T_f) and cold permeate (T_c) are the most affecting parameters on the DCMD system performance, Figs. 7 and 8 show, experimentally and theoretically, the effects of the temperature difference and temperature ratio between the hot feed and cold permeate streams; respectively. The operating conditions are; PTFE membrane with pore size of 0.45 μm, feed flow rate 4.65 L/min, cold permeate flow rate of 3.65 L/min. The feed is seawater with

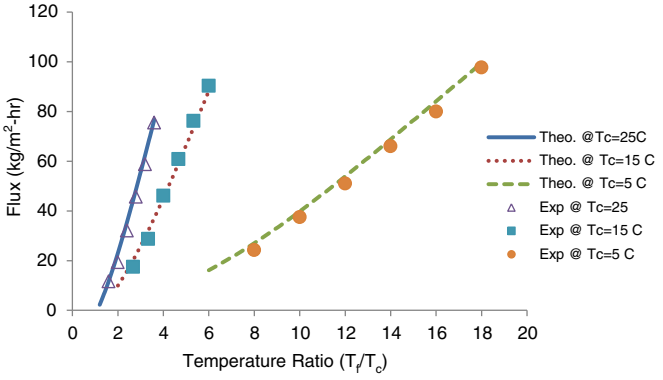

Fig. 8. Effect of operating temperature ratio on flux.

concentration of 43 g/L. The plots are produced for different selected cold permeate temperatures of 5, 15, and 25 °C.

From Figs. 7 and 8, good agreements are observed between theoretical and experimental values of flux at different operating combinations of feed and cold permeate temperatures differences and ratios. These good agreements attest the reliability of the analytical model to predict the system flux under different conditions. Of course, increasing the temperature difference increases the flux as shown in Fig. 7. However, at a given temperature difference, higher cold permeate temperature yields higher flux. This behavior may be attributed to the large conduction heat loss across the membrane and from the module itself to the surroundings at lower temperature of the cold permeate stream. From Fig. 8, when the temperature ratio increases, the flux increase exponentially and the variation trends have different slopes corresponding to different temperatures of the cold permeate. The curves slopes tend to decrease as the cold permeate temperature decreases from 25 °C to 5 °C. It is interesting to know that in order to produce 60 kg/m^2·h of distillate, for example from Fig. 8, one needs to set the feed temperature at 80 °C if the cold side temperature is 25 °C, 70 °C if the cold side is at 15 °C, and 64 °C if the cold side is at 5 °C. One may conclude that utilizing energy for heating the feed side water is more efficient (produces more flux) than utilizing the same amount of energy for cooling the cold stream. More specifically, use energy for heating while using room temperature water for the cold permeate stream.

4.2. Effect of feed and cold permeate flow rates

When the flow rate increases the channel flow Reynolds number increases, and hence the turbulence level. The direct outcome is to enhance the mixing in the boundary layer adjacent to the membrane surface leading to higher heat and mass transfer coefficients. In DCMD modules, both feed and permeate streams are in direct contact with the membrane and thus the flow rates on both membrane sides are expected to be effective on permeation process. Fig. 9 shows the effect of feed flow rate on the system permeate flux. The increase in flux is prominent with increasing the feed flow rate. For instant, at feed temperature of 90 °C, permeate flux increases from 55 to 72 kg/m^2·h, by increasing the flow rate from 2.5 to 4.6 L/min, which is about 31% increase. The corresponding percentage increase in flux, for the same change in feed flow rate, at feed temperatures of 50 °C and 70 °C is found to be about 28%. If one looks from the feed temperature point of view, increasing the feed temperature from 50 °C to 90 °C yields about 260% increase in flux at feed flow rate of 2.5 L/min and about 290% at feed flow rate of 4.6 L/min. This result indicates that increasing the feed flow rate is more effective in improving the flux at higher feed temperatures in particular. The channel flow Reynolds number in feed side was found to be turbulent (>2300) for the considered conditions of feed flow rate and temperature. On the other hand, increasing the turbulence level reduces the residence time of the feed water in the feed channel. The effect of residence time on permeate flux is implanted in the flow rate and turbulence effects and needs more investigations in future.

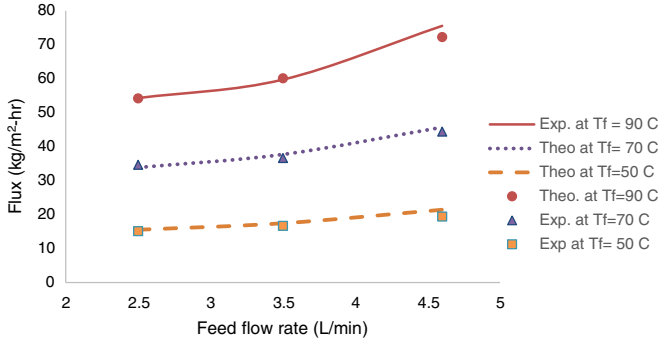

Fig. 9. Effect of feed flow rate on the permeate flux. Operating conditions: coolant flow rate 3.65 L/min, feed temperature 90 °C, coolant temperature 25 °C.

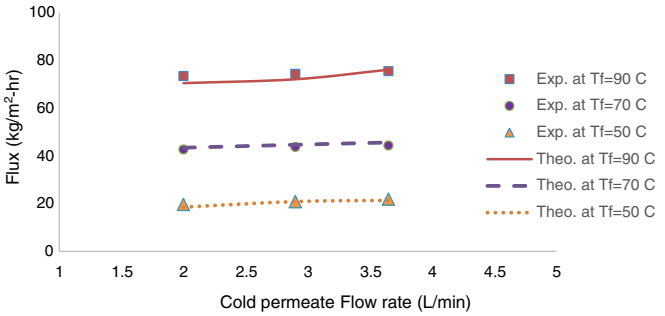

Fig. 10. Effect of coolant flow rate on permeate flux. Operating conditions: PTFE membrane, 0.45 μm, permeate temperature 25 °C, feed flow rate 4.65 L/min, feed concentration 2 g/L.

Fig. 10 shows that permeate flux increases with increasing the flow rate of the cold permeate stream, at selected different feed temperatures of 50, 70, and 90 °C. Increasing the coolant flow rate from 2 to 3.65 L/min (laminar channel flow, $Re < 2300$ for all tested cases) resulted in only 4.6% increase in permeate flux at feed temperature of 90 °C and this percentage increases to 11% for feed temperature of 50 °C. Increasing the cold permeate flow rate is less effective on the permeate flux as compared to the effect of increasing the feed flow rate. The feed side is always more effective on the permeate flux since it is the source vaporization and controlling the permeation process.

Fig. 11 shows the effect of the ratio between feed flow rate and cold permeate flow rate (V_f/V_p) on flux both experimentally and theoretically, for selected permeate flow rates (namely, V_p = 2, 2.9 and 3.65 L/min). The test conditions are: PTFE 0.45 μm membrane, inlet feed temperature of 90 °C, inlet permeate temperature of 25 °C, feed concentration of 43 g/L, and the feed flow rate is varied from 2.5 L/min to 4.65 L/min. It is observed that increasing the flow ratio (V_f/V_p) increases the flux at any cold permeate flow rate in a parabolic manner. For a given ratio, higher permeate flow rate yields considerable increase in flux output. In addition, a good coherence is observed between theoretical values and experimental values of flux at all permeate flow rate.

4.3. Effect of feed concentration

To study the effect of feed concentration on the flux of the DCMD system, four levels of feed concentrations are tested as mentioned above in Section 3, namely 0.14, 2, 43, and 100 g/L. these values were selected to cover a wide range of feed concentrations from very low to very high values including the seawater of 43 g/L. The test conditions are: feed flow rate 4.65 L/min, coolant flow rate 3.65 L/min, and cold permeate temperature of 25 °C. Fig. 12 shows that the permeate flux is continuously decreasing as the feed salinity increases. The flux

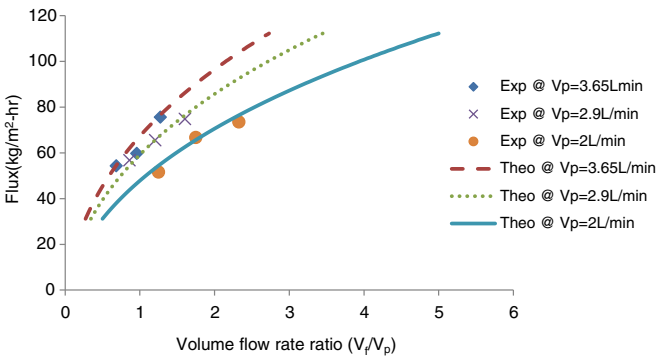

Fig. 11. Effect of flow rate ratio (feed/permeate) on flux.

$$SRF = \frac{Feed\ Concentration - Permeate\ Concentration}{Feed\ Concentration} x100 \quad (37)$$

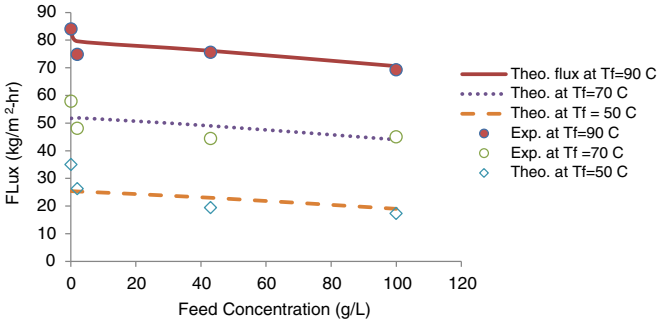

Fig. 12. Influence of feed concentration of flux. Conditions: membrane PTFE 0.45 μm, cold permeate temperature 25 °C, feed flow rate 4.65 L/min, cold permeate flow rate 3.65 L/min.

reduction with increasing the feed concentration is mainly due to the increasing effect of the salt concentration polarization, which adds more resistance to vapor permeation across the membrane. In addition, scaling and fouling on the membrane surface due to salts and impurities tend to cover some effective area of membrane that retards the evaporation process and reduces the vapor pressure difference across the membrane, so ultimately the flux decreases. Few conclusions may be extracted from Fig. 12: The decrease in flux follows linear decreasing trend with increasing the feed concentration. The DCMD system is able to handle feed solutions with high concentration of 100 g/L, which attests its ability to desalinate brine solutions of high concentration, like oilfield produced water for example, as mentioned by [11]. In calculating the percentage reduction in flux when increasing the feed concentration from 0.14 to 100 g/L, about 50% reduction in flux at feed temperature of 50 °C, 22% reduction at 70 °C, and 17.5% reduction at 90 °C is achieved. Therefore, it is obvious that the effect of feed concentration is becoming less significant at high feed temperature as compared to operating at low feed temperature.

Salt rejection factor (SRF) is a measure of the quality of the flux and the efficiency of separation process. It is defined as;

$$SRF = \frac{Feed\ Concentration - Permeate\ Concentration}{Feed\ Concentration} \times 100 \quad (37)$$

Fig. 13 shows the SRF values for different feed concentrations at different feed temperatures. Four levels of feed concentrations, 0.140, 2, 43 and 100 g/L are tested. For low feed concentration of 0.14 g/L, the salt rejection factor was 97.8%. As the feed concentration increases from 0.14 to 2 g/L, the SRF increased to 99.15%. When seawater (43 g/L) and the extreme concentration NaCl solution of 100 g/L are used as feed, the salt rejection factor was 99.96%. These high values of the SRF indicate

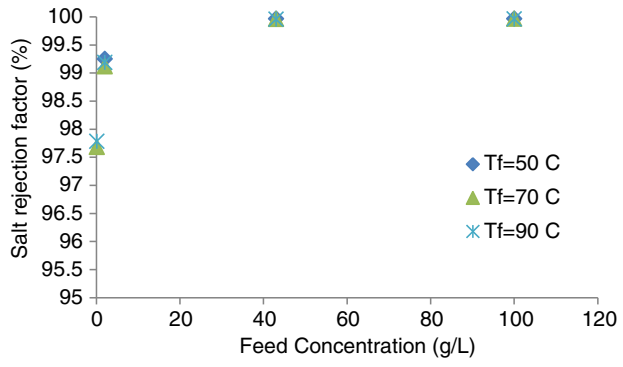

Fig. 13. Influence of feed concentration on quality of permeate. Operating conditions: PTFE 0.45 μm, feed flow rate 4.65 L/min, cold permeate flow rate 3.65 L/min.

the effectiveness of the DCMD systems in handling seawater and high concentrations feeds for water desalination. More details and discussion on this point are presented later in Section 4.4, Fig. 19.

4.4. Effect of membrane pore size and degradation

The MD separation performance is directly associated with the overall membrane morphology, which is considered the most important component of the MD process. Therefore, the successful application of MD may be aided by a good knowledge of the different membrane parameters. Two polytetrafluoroethylene (PTFE) membranes, acquired from Tisch Scientific Corporation, with different pore sizes were used in the present study, namely PTFE SF17385 and SF17386 membranes with mean pore sizes of 0.22 μm and 0.45 μm; respectively as reported by the manufacturer. It is worth noting that PTFE membrane is composed of two layers, a thin active layer and a support layer. The characterization of the two membranes used in the present work was carried out in our labs and the measured values are listed in Table 1. The measured properties included the actual overall thickness ($\delta_{membrane}$), the active layer thickness (δ_{active}), the mean pore size (d_p), the porosity (ε), the water contact angle (θ), and the liquid water entry pressure (LEP). More details on membrane characterization can be found in Khalifa et al. [41].

Fig. 14 shows SEM micrographs of top (active) surface taken from both PTFE (0.22 μm) and PTFE (0.45 μm) membranes, while Fig. 15 displays SEM micrographs of their respective cross sections. The active layer of both membranes is of about the same thickness, as well as their overall thickness. Moreover, they also display similar values of the porosity and degree of hydrophobicity, rendering the comparison useful with respect to their flux performance. It is worth indicating that according to our measurements, the PTFE (0.45 μm) membrane exhibits an overall lower average pore size than that reported by the supplier that is roughly 0.38 μm (measured) compared to 0.45 μm (reported). As expected, the LEP of PTFE (0.22 μm) membrane is slightly higher than that of PTFE (0.45 μm).

Membrane pore size is an important property of the membrane morphology. Bigger pore size means less resistance to mass transfer and hence higher driving force for permeation across the membrane. Fig. 16 shows that the PTFE (0.45 μm) membrane produces a relatively higher flux compared to PTFE (0.22 μm) membrane. Regarding the effect of feed temperature (40 to 90 °C) on the percentage flux increase between the two membranes, there is an average of 7 to 9% flux increase, except for a jump of 20% flux increase at 80 °C. This indicates a general consistent percentage flux increase for the larger pore size at different feed temperatures. Another important note from Fig. 16 is that almost doubling the membrane pore size does not lead to doubling the flux, indicating the nonlinearity behavior between the flux and pore size. As mentioned earlier, both membranes have similar active layer and overall thicknesses, close values of the porosity, and similar degrees of hydrophobicity. Usually, the pore size of commercial membranes is not exceeding 1 μm. For pore sizes > 1 μm, surface energy of membrane materials decreases, and hydrophobicity decreases, leading to pore wetting phenomenon and hence deteriorating the MD process performance [27]. The theoretical model results indicate a consistent flux

Table 1
Measured properties of the PTFE membranes.

Membrane type	Membrane characteristics					
	$\delta_{membrane}$ (μm)	δ_{active} (μm)	d_p (nm)	ε (%)	θ (°)	*LEP* (bar)
PTFE-SF17385 (0.22 μm)	159 ± 18	8 ± 2	236 ± 6	76 ± 5	138 ± 2	3.3 ± 0.1
PTFE-SF17386 (0.45 μm)	154 ± 14	7 ± 2	379 ± 8	80 ± 9	139 ± 3	2.4 ± 0.1

($\delta_{membrane}$: membrane thickness, δ_{active}: thickness of membrane active layer, d_p: mean pore size, ε: porosity, θ: water contact angle, LEP: liquid water entry pressure).

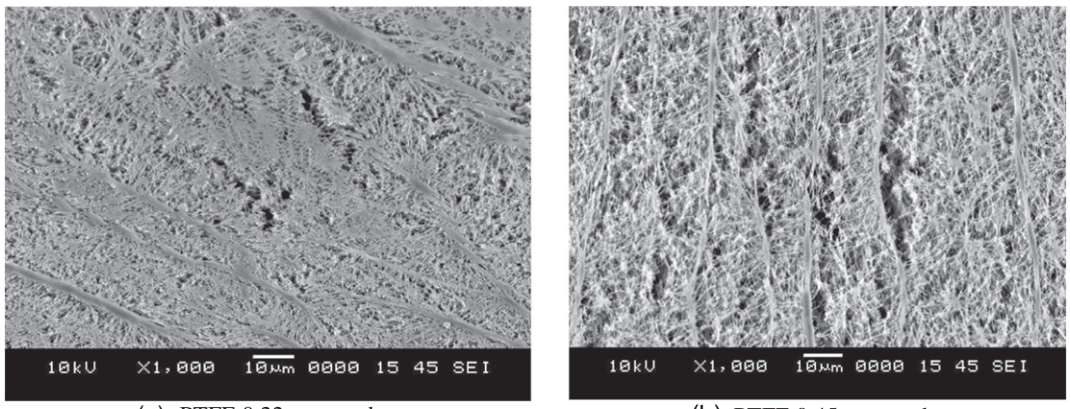

(a) PTFE 0.22µm membrane (b) PTFE 0.45µm membrane

Fig. 14. SEM micrographs of top surface taken from as-received PTFE (0.22 µm) and PTFE (0.45 µm) membranes.

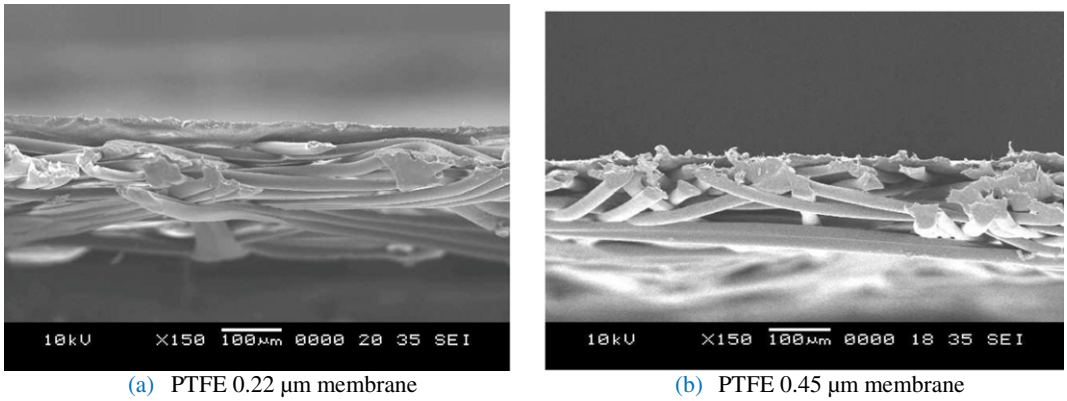

(a) PTFE 0.22 µm membrane (b) PTFE 0.45 µm membrane

Fig. 15. SEM micrographs of cross sections taken from PTFE (0.22 µm) and PTFE (0.45 µm) membranes.

enhancement when using larger pore size for the whole range of feed temperatures and agree well with the experimental results.

A continuous 48-h experiment was conducted to investigate the effect of continuous operation of the system on permeate flux and membrane degradation. Fig. 17 shows the variation in permeate flux with time over the 48 h. The experiment was performed using the PTFE 0.45 membrane, with two types of feed water of different concentrations, namely sweet tap water (0.14 g/L) and seawater (43 g/L). Feed flow rate is set at 3.75 L/min and cold permeate flow rate at 3.65 L/min. For the tap water, the maximum flux is obtained at the start of the experiment, followed by a noticeable decrease in flux after 3 h, thereafter remaining almost constant for the rest of the test period with minor perturbations. In general, about 15% reduction in flux was recorded over the 48 h period. On the other hand, the use of seawater as feed gave different results. First, as expected, the seawater flux is lower than that of tap water due to its higher concentration. Second, a sharp and continuous reduction in flux was recorded after 20 h, yielding an average percentage reduction in flux after of 42% after 48 h. This large reduction in flux with time for seawater can be attributed to the effect of salt precipitation and fouling on the membrane surface, in addition to

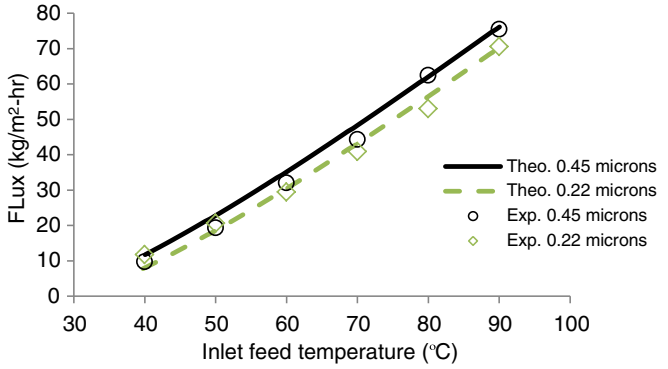

Fig. 16. Effect of membrane pore size on permeate flux Conditions: permeate temperature 25 °C, feed flow rate 4.65 L/min, cold permeate flow rate 3.65 L/min, and feed concentration 43 g/L.

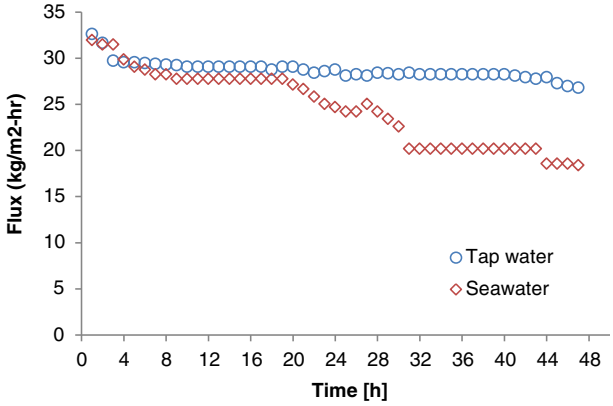

Fig. 17. Seawater and tap water flux variation versus time Conditions: PTFE 0.45 µm, feed flow rate 3.75 L/m, coolant flow rate3.65 L/min, feed temperature 60 °C, coolant temperature 20°.

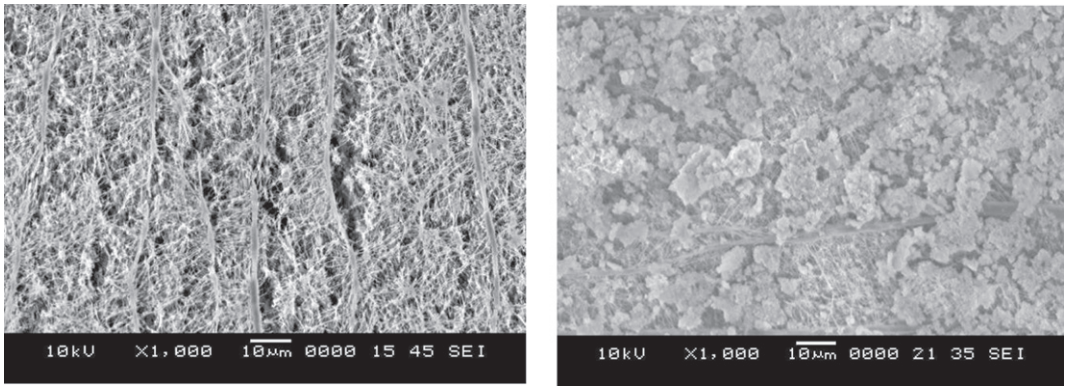

(a) New PTFE 0.45 µm membrane (b) Used PTFE 0.45 µm membrane

Fig. 18. SEM micrographs of PTFE (0.45 µm) membrane, (a) as-received, and (b) after 48 h continuous flow test operation.

the concentration polarization. Indeed, the membrane degradation after the 48 h continuous flow operation is clearly visible in Fig. 18b which displays the SEM image of the used PTFE (0.45 µm) membrane covered with a fouling layer, as compared to the as-received membrane shown in Fig. 18a. According to the flux results shown in Fig. 17, the fouling layer may have started its formation (most probably covering a large portion of the membrane surface) after about 20 h flow test operation due to the noticeable decrease in the flux. Longer testing led to further membrane degradation resulting in almost 50% flux decrease after 48 h. Longer testing data are not available.

Fig. 19a shows the variation of salt rejection factor with time. For tap water, at the beginning of the experiment the salt rejection factor is almost 98% and went on decreasing with the passage of time reaching 96.7% at the end of the experiment. In agreement with Fig. 17, the salt rejection factor decreased in the first few hours, remained constant for another 6 h, and repeated the same behavior as time advances. The change in the salt rejection factor in this case was 3.4%. For seawater, salt rejection factor started at 99.98% and became 99.956% at the end of the experiment, which is only 0.04% change in the rejection factor over 48 h. Fig. 19 proves the consistency of DCMD configuration for seawater desalination. One may question the higher rejection factor for seawater compared to sweet tap water. It should be mentioned that the TDS of distillate water, used in the permeate side to start the experiment, is not exactly zero; it was measured to be about 2 to 3 mg/L. With operation, The TDS of the permeate side increases slightly with time; as shown in Fig. 19b. The permeate TDS for tap water may be considered constant in the range of 4 to 5 mg/L over the 48 h. On the other hand, the permeate TDS of seawater feed changed from 7 mg/L at the beginning of the experiment to 20 mg/L after 48 h. However, the TDS of feed seawater (43,000 mg/L) is very high compared to the TDS of tap water (140 mg/L) and the ratio in the definition of the salt rejection factor presented in Eq. (37) yields the results shown in Fig. 19a.

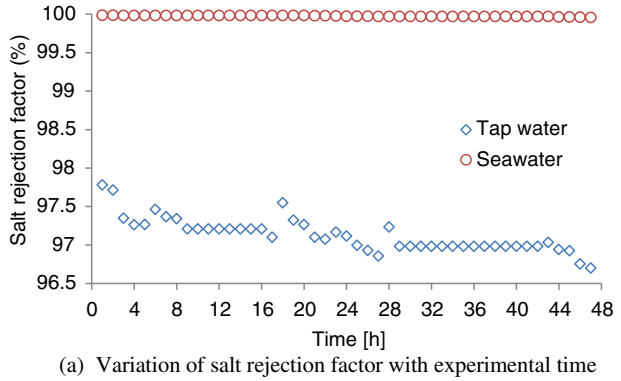

(a) Variation of salt rejection factor with experimental time

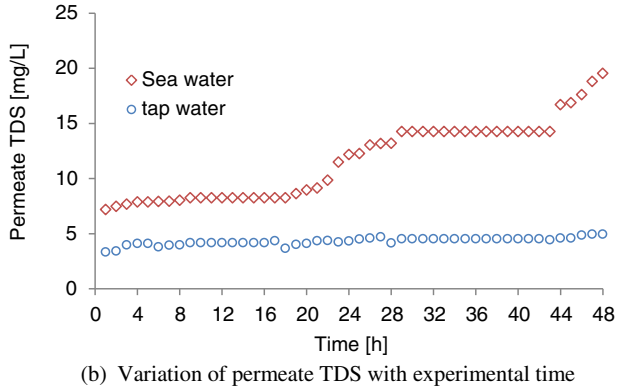

(b) Variation of permeate TDS with experimental time

Fig. 19. Variations of flux quality measures of the DCMD system with time. (a) Variation of salt rejection factor with experimental time (b)Variation of permeate TDS with experimental time.

4.5. Energy analysis

The evaporative (thermal) efficiency, *EE*, is defined as the ratio of evaporative heat transfer to the total heat transferred to the membrane (or through MD module) and is be given as [40,41]

$$\%EE = \left(\frac{Q_v}{Q_m}\right) * 100 = \left(\frac{J_w * \Delta H_v}{U * (T_{b,f} - T_{b,p})} * 100\right) \quad (38)$$

From Fig. 20, the evaporative efficiency ranged from 70% to 95% corresponding to feed temperature from 40 °C to 90 °C. Increasing the inlet feed temperature increases the evaporative efficiency due to flux increasing. Another interesting behavior shown in Fig. 20 is that the evaporative efficiency is higher at higher cold permeate temperature, for a given feed temperature. In terms of percentage change it can be observed that at 40 °C, the increase in evaporative efficiency is 12.63% when the bulk coolant (permeate) temperature, Tbc, is changed from 5 °C to 25 °C. However, as the inlet feed temperature increases, the differences in the efficiency values diminish, and at 90 °C, it is 2% only. Thus, when operating the DCMD system at higher feed temperature, the effect of inlet coolant temperature on the efficiency is not significant. However, if the system is running at low inlet feed temperature then higher inlet coolant temperature is preferred for higher evaporative efficiency.

The gain output ratio (GOR) is another performance measure that is used extensively in thermal desalination to assess the thermal process energy efficiency. The MD technique is mainly thermal (evaporation

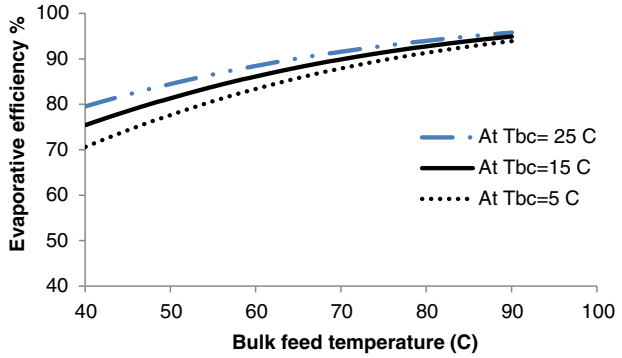

Fig. 20. Effect of feed temperature on evaporative efficiency. Operating conditions: PTFE 0.45 μm, feed flow rate 4.65 L/m, coolant flow rate 3.65 L/m, feed concentration 140 mg/L, coolant temperature T_{bc} = 5,15,25 °C.

in the feed side and condensation in the permeate/cold side) and the permeation is mainly due to the applied temperature difference across the membrane. Thus, GOR definition can be applied to MD systems [43,44]. The GOR value may be of interest with MD practically to compare its progress with other common desalination techniques like thermal ones. The GOR definition is even used with the RO system which is not thermal in nature, when combined with MD system, [45]. It is defined as the ratio of latent heat of vaporization of the distillate produced to the heat input to the system with the feed stream [39,42–45];

$$GOR = \frac{m_d * \Delta H_v}{\dot{m}_f * c_{pf} * \Delta T_{module}} \tag{39}$$

where $m_d$is the mass of the produced permeate, ΔH_v is the latent heat of vaporization, $\dot{m}_f$is mass flow rate of feed water, $c_{pf}$is the specific heat of feed, and $\Delta T_{module}$is the temperature difference between inlet and outlet of hot side of module.

Fig. 21 shows the variation of the GOR value with inlet feed temperature, at different cold permeate temperatures of 5, 15 and 25 °C. The GOR calculated values increases with increasing the inlet feed temperature up to 60 °C then decreases with increasing feed inlet temperature up to 90 °C. Experiments shows that working at higher cold permeate temperature results in higher values of GOR than operating at lower cold permeate temperatures. In addition, the temperature difference between inlet and outlet of hot side of module, ΔT_{module}, is increasing exponentially as the feed temperature increases, resulting in lower GOR values. The GOR values were between 0.8 and 1.2 for the tested range of feed temperature, for the used DCMD system.

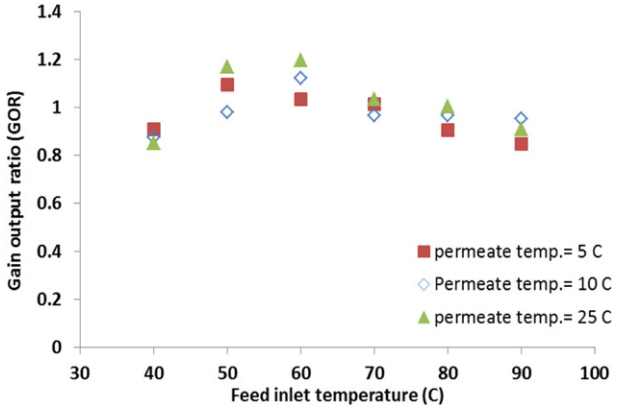

Fig. 21. Effect of feed inlet temperature on gain output ratio [39] *Conditions*: PTFE 0.45 μm membrane, feed flow rate 4.65 L/min, permeate flow rate 3.65 L/min, feed salinity 2 g/L.

5. Conclusion

A comprehensive study of the performance of the DCMD system was presented. Details of the experimental setup and the DCMD module design and assembly were provided. Main variables affecting the system performance and degradation were discussed both experimentally and analytically. The membranes used in the study were characterized and the effects of long-term operation on the membrane surface and system performance were studied. The analytical model is based on solving the equations of heat and mass transfer with the DCMD module. The developed model has proven its ability to predict the system performance at different operating conditions with maximum deviations of <10% from experimental measurements. The investigated variables included feed temperature, cold permeate temperature, feed-permeate temperature difference and ratio, feed flow rate, permeate flow rate, feed-permeate flow rate ratio, feed concentration, membrane pore size, and membrane degradation with time. Permeate flux increases, almost exponentially, as the feed temperature increases. Nevertheless, it increases almost linearly as the permeate temperature decreases. The effect of decreasing the permeate temperature is smaller than the effect of increasing the feed temperature. This indicates that the system is better operated at high feed temperatures while saving the cooling energy by running the permeate at ambient temperature. The permeate flux also increases with the flow rate of both feed and permeate. High flow rates generate more turbulence thus enhancing the heat and mass transfer. The effects of feed flow rate are more notable at high feed temperature. The DCMD system is able to handle feeds with high salt concentration of 100 g/L with remarkably high salt rejection factor and low permeate TDS. However, the recorded flux reduction was between 17 and 50% depending on the feed temperature, showing that operating at high feed temperature results in less reduction in flux when using high feed concentration. An average of about 8% increase in flux was obtained when the pore size of the PTFE membrane was increased from 0.22 to 0.45 μm. The SEM micrographs revealed that the used PTFE membrane being covered with a fouling layer, as compared to the as-received (new) membrane, and the fouling phenomena may have started its formation after about 20 h flow test operation as indicated by the noticeable decrease in the flux. The evaporative efficiency ranged from 70% to 95% corresponding to feed temperature from 40 °C to 90 °C and the calculated GOR values were between 0.8 and 1.2 for the same range of feed temperature.

Acknowledgement

The authors acknowledge the support and fund received from the Deanship of Research, King Fahd University of Petroleum & Minerals (KFUPM) under Research Grant # IN141035.

References

[1] B.D. Negewo, Renewable Energy Desalination: An Emerging Solution to Close the Water Gap in the Middle East and North Africa, World Bank Publications, 2012.
[2] http://environment.nationalgeographic.com/environment/freshwater/freshwater-crisis/,Fresh Water Crisis.
[3] K.C. Ng, K. Thu, Y. Kim, A. Chakraborty, G. Amy, Adsorption desalination: an emerging low-cost thermal desalination method, Desalination 308 (2013) 161–179.
[4] K. Thu, A. Chakraborty, Y.D. Kim, A. Myat, B. Saha, K.C. Ng, Numerical simulation and performance investigation of an advanced adsorption desalination cycle, Desalination 308 (2013) 209–218.
[5] C.J. Vörösmarty, P.B. McIntyre, M.O. Gessner, D. Dudgeon, A. Prusevich, P. Green, P.M. Davies, Global threats to human water security and river biodiversity, Nature 467 (7315) (2010) 555–561.
[6] R. Smalley, N. Laureate, Seawater Desalination, Department of Chemical and Environmental Engineering, Yale University Menachem Elimelech, 2012.
[7] R.P. Singh, Water desalination: the role of RO and MSF, IOSR J. Environ. Sci., Toxicol. Food Technol.(IOSR-JESTFT) (2013) 1–65.
[8] A. Mabrouk, Techno-economic analysis of tube bundle orientation for high capacity brine recycle MSF desalination plants, Desalination 320 (2013) 24–32.
[9] T. Mezher, H. Fath, Z. Abbas, A. Khaled, Techno-economic assessment and environmental impacts of desalination technologies, Desalination 266 (1) (2011) 263–273.

[10] Ó. Andrjesdóttir, C.L. Ong, M. Nabavi, S. Paredes, A.S.G. Khalil, B. Michel, D. Poulikakos, An experimentally optimized model for heat and mass transfer in direct contact membrane distillation, Int. J. Heat Mass Transf. 66 (2013) 855–867.
[11] F. Macedonio, A. Ali, T. Poerio, E. El-Sayed, E. Drioli, M. Abdel-Jawad, Direct contact membrane distillation for treatment of oilfield produced water, Sep. Purif. Technol. 126 (2014) 69–81.
[12] Y.M. Manawi, M.A. Khraisheh, A.K. Fard, F. Benyahia, S. Adham, A predictive model for the assessment of the temperature polarization effect in direct contact membrane distillation desalination of high salinity feed, Desalination 341 (2014) 38–49.
[13] S.T. Hsu, K.T. Cheng, J.S. Chiou, Seawater desalination by direct contact membrane distillation, Desalination 143 (3) (2002) 279–287.
[14] A. Boubakri, A. Hafiane, S. Bouguecha, Direct contact membrane distillation: capability to desalt raw water, Arab. J. Chem. (2014), http://dx.doi.org/10.1016/j.arabjc.2014.02.010.
[15] S. Lin, N.Y. Yip, M. Elimelech, Direct contact membrane distillation with heat recovery: thermodynamic insights from module scale modeling, J. Membr. Sci. 453 (2014) 498–515.
[16] S. Srisurichan, R. Jiraratananon, A.G. Fane, Mass transfer mechanisms and transport resistances in direct contact membrane distillation process, J. Membr. Sci. 277 (1) (2006) 186–194.
[17] G. Naidu, S. Jeong, S. Vigneswaran, Influence of feed/permeate velocity on scaling development in a direct contact membrane distillation, Sep. Purif. Technol. 125 (2014) 291–300.
[18] C.D. Ho, C.H. Huang, F.C. Tsai, W.T. Chen, Performance improvement on distillate flux of countercurrent-flow direct contact membrane distillation systems, Desalination 338 (2014) 26–32.
[19] M. Qtaishat, T. Matsuura, B. Kruczek, M. Khayet, Heat and mass transfer analysis in direct contact membrane distillation, Desalination 219 (1) (2008) 272–292.
[20] D. Lawal, A. Khalifa, Flux prediction in direct contact membrane distillation, Int. J. Mater. Mech. Manuf. 2 (4) (2014) 302–308.
[21] Z. Ding, R. Ma, A.G. Fane, A new model for mass transfer in direct contact membrane distillation, Desalination 151 (3) (2003) 217–227.
[22] L. Martinez, F.J. Florido-Diaz, Theoretical and experimental studies on desalination using membrane distillation, Desalination 139 (1) (2001) 373–379.
[23] M. Khayet, Membranes and theoretical modeling of membrane distillation: a review, Adv. Colloid Interf. Sci. 164 (1) (2011) 56–88.
[24] M. Essalhi, M. Khayet, Self-sustained webs of polyvinylidene fluoride electrospun nanofibers at different electrospinning times: 2. Theoretical analysis, polarization effects and thermal efficiency, J. Membr. Sci. 433 (2013) 180–191.
[25] Z.W. Song, L.Y. Jiang, Optimization of morphology and perf ormance of PVDF hollow fiber for direct contact membrane distillation using experimental design, Chem. Eng. Sci. 101 (2013) 130–143.
[26] T.C. Chen, C.D. Ho, H.M. Yeh, Theoretical modeling and experimental analysis of direct contact membrane distillation, J. Membr. Sci. 330 (1) (2009) 279–287.
[27] M. Khayet, T. Matsuura, Membrane Distillation: Principles and Applications, Elsevier, 2011.
[28] J. Phattaranawik, R. Jiraratananon, A.G. Fane, Effect of pore size distribution and air flux on mass transport in direct contact membrane distillation, J. Membr. Sci. 215 (1) (2003) 75–85.
[29] S.B. Iversen, V.K. Bhatia, K. Dam-Johansen, G. Jonsson, Characterization of microporous membranes for use in membrane contactors, J. Membr. Sci. 130 (1) (1997) 205–217.
[30] A. Alkhudhiri, N. Darwish, N. Hilal, Membrane distillation: a comprehensive review, Desalination 287 (2012) 2–18.
[31] Y. Yun, R. Ma, W. Zhang, A.G. Fane, J. Li, Direct contact membrane distillation mechanism for high concentration NaCl solutions, Desalination 188 (1) (2006) 251–262.
[32] J. Phattaranawik, R. Jiraratananon, A.G. Fane, Heat transport and membrane distillation coefficients in direct contact membrane distillation, J. Membr. Sci. 212 (1) (2003) 177–193.
[33] L. Francis, N. Ghaffour, A.A. Alsaadi, G.L. Amy, Material gap membrane distillation: a new design for water vapor flux enhancement, J. Membr. Sci. 448 (2013) 240–247.
[34] L. Martínez-Díez, F.J. Florido-Díaz, M.I. Vázquez-González, Study of polarization phenomena in membrane distillation of aqueous salt solutions, Sep. Sci. Technol. 35 (10) (2000) 1485–1501.
[35] L. Martínez-Díez, M.I. Vazquez-Gonzalez, Temperature and concentration polarization in membrane distillation of aqueous salt solutions, J. Membr. Sci. 156 (2) (1999) 265–273.
[36] S. Srisurichan, R. Jiraratananon, A.G. Fane, Mass transfer mechanisms and transport resistances in direct contact membrane distillation process, J. Membr. Sci. 277 (1) (2006) 186–194.
[37] K.W. Lawson, D.R. Lloyd, Membrane distillation, J. Membr. Sci. 124 (1) (1997) 1–25.
[38] Y.M. Manawi, M. Khraisheh, A.K. Fard, F. Benyahia, S. Adham, Effect of operational parameters on distillate flux in direct contact membrane distillation (DCMD): comparison between experimental and model predicted performanc, Desalination 336 (2014) 110–120.
[39] H.M. Ahmad, A.E. Khalifa, M.A. Antar, Performance of direct contact membrane distillation system for water desalination, ASME International Mechanical Engineering Congress & Exposition, *IMECE-2015*, Paper No. IMECE2015–50171 Houston, Texas, USA, November 13–19 2015.
[40] J. Zhang, S. Gray, Predicting the influence of operating conditions on DCMD flux and thermal efficiency for incompressible and compressible membrane systems, Desalination 323 (2013) 142–149.
[41] A. Khalifa, D. Lawal, M. Antar, M. Khayet, Experimental and theoretical investigation on water desalination using air gap membrane distillation, Desalination 376 (2015) 94–108.
[42] P.N. Govindan, Status of Humidification Dehumidification Desalination Technology, International Desalination Association Journal, World Water Congress, Perth, Australia, 2011.
[43] R.B. Saffarini, E.K. Summers, H.A. Arafat, John H, Lienhard V, Technical evaluation of stand-alone solar powered membrane distillation systems, Desalination, Volume 286 (2012) 332–341.
[44] E.K. Summers, H.A. Arafat, J.H. Lienhard V, Energy efficiency comparison of single-stage membrane distillation (MD) desalination cycles in different configurations, Desalination 290 (2012) 54–66.
[45] H. Geng, J. Wang, C. Zhang, P. Li, H. Chang, High water recovery of RO brine using multi-stage air gap membrane distillation, Desalination 355 (1) (January 2015) 178–185.

Nomenclature

A: Area, m^2
C_p: Specific heat J/kg-K
D_h: Hydraulic diameter, m
D_{pore}: Pore diameter, m
D_e: Diffusion coefficient, m^2/s
%EE: Percent evaporative efficiency
h: Convective heat transfer coefficient W/m^2-K
ΔH: Enthalpy or Latent Heat of vaporization of water, kJ/kg
k: Thermal conductivity, W/m-K
k_s: Solute mass transfer coefficient, m/s
Mol: Molecular weight g/mol
J_w: Mass flux kg/m^2-s
k_b: Boltzman constant, 1.3807×10^{-23} J/K
K_n: Knudsen number
P: Pressure, Pa
Q: Heat transfer, W/m^2
r: Radius of membrane pore, m
R: Universal gas constant, 8314 J/kmol-K
Nu: Nusselt number
Re: Reynolds number
Sc: Schmidt number
Sh: Sherwood number
T: Absolute temperature, K
U: Overall heat transfer coefficient, W/m^2-K
x: Mole fraction

Greek symbols

α: Contribution of knudsen diffusion to mass transfer
β: Concentration Polarization coefficient
δ: Membrane thickness, m
ε: Porosity, %
μ: Viscosity Pa-s
ρ: Density kg/m^3
γ: Salt activity coefficient
τ: Membrane tortuosity
λ: Mean Free path of water molecule, (m)

Subscripts

Ch.: Channel
F: Feed side
p: Permeate side
bf: bulk Feed
bp: bulk Permeate
mf: Membrane feed side
mp: Membrane permeate side
c: Conduction
m: membrane
mem.: membrane material
k: Knudsen
M: Molecular
V: Vapors/Vaporization
w: Water
w-a: Water in Air
w,v,p: Water Vapors inside the pores